IEEE Access
Multidisciplinary | Rapid Review | Open Access Journal

SPECIAL SECTION ON TRENDS, PERSPECTIVES AND PROSPECTS OF MACHINE LEARNING APPLIED TO BIOMEDICAL SYSTEMS IN INTERNET OF MEDICAL THINGS

Received May 26, 2018, accepted July 2, 2018, date of publication July 23, 2018, date of current version August 15, 2018.

Digital Object Identifier 10.1109/ACCESS.2018.2856244

Automatical Intima-Media Border Segmentation on Ultrasound Image Sequences Using a Kalman Filter Snake

SHEN ZHAO[1,2], GUANGRUI LI[1], WEI ZHANG[1], (Member, IEEE), AND JIANJUN GU[1]

[1]School of Control Science and Engineering, Shandong University, Jinan 250061, China
[2]Department of Medical Biophysics, The University of Western Ontario, London, ON N6A 3K7, Canada

Corresponding author: Wei Zhang (davidzhang@sdu.edu.cn)

This work was supported in part by NSFC under Grant 61573222, in part by the Major Research Program of Shandong Province under Grant 2018CXGC1503, in part by the Shenzhen Future Industry Special Fund under Grant JCYJ20160331174228600, in part by the Science Technology and Innovation Committee of Shenzhen for Research Projects under Grant JCYJ20170413114916687 and Grant SGLH20161212104605195, and in part by the Fundamental Research Funds of Shandong University under Grant 2016JC014.

ABSTRACT Segmentation of carotid intima-media (IM) borders from ultrasound images is of great importance for predicting cardiovascular risks. In this paper, we have developed a fully automatic approach to sequentially segment the carotid IM borders in each image throughout ultrasound sequences. First, the first frame of an ultrasound sequence is automatically segmented using edge detectors and dynamic programming, and then the rest frames are segmented successively under the state-space framework. Under this framework, we developed a variant of the snake method for a precise measurement. The evaluation of our segmentation result is done by comparison with average manual delineations of three physicians on a total of 65 sequences. The accuracy of our method is high. (Segmentation error is 32.1 ± 37.5 μm for LI and 35.0 ± 41.5 μm for MA.) The BA plot and the linear regression also demonstrate that our method is in agreement with the ground truth. This paper strengthens the potential of the state-space and snake-based approach in segmenting IM borders for clinical diagnosis by demonstrating a fully automatic scheme.

INDEX TERMS Snake, Kalman, state-space framework, carotid intima-media (IM) borders, sequence segmentation.

I. INTRODUCTION

Atherosclerosis give rise to lethal cardiovascular illnesses, for example, coronary heart disease and cerebral infarction, which causes thousands of deaths each year [1]. A number of studies show that carotid intima-media thickness (IMT) is commonly used to predict atherosclerotic diseases [2]–[4]. It is reported that the artery is healthy when IMT is smaller than 1.1mm, while the artery is at risk when IMT is larger than 1.5mm [5], [6]. Ultrasound imaging is usually used to examine the biomechanical dynamics of carotid intima-media [7], and resultantly, IMT measurement can be achieved by segmentation of ultrasound images.

Previously, segmentation of ultrasound images has been extensively studied by different teams for assessing IMT at the early stage of atherosclerosis [8]–[10]. A novel multi-ethnic research recently reveals the strong relationship between the IMT variation and the probability of cardiovascular event developments [11]. The correlation of IMT change and cardiovascular risks is still open to discussion, so the observation of IMT variation during the cardiac cycle becomes an important issue. Thus, the task of IM segmentation during the cardiac cycle receives more and more recognition in recent years [3]. However, this is still very challenging because of large observer viability, noisy ultrasound images, and carotid plaques in ultrasound data [12]–[14]. Also, fully automated methods for segmentation of ultrasound sequences should be developed to maximally limit the workload of the users [12].

In computer-aided IM segmentation, the IM borders (which contains the lumen-intima border and the media-adventitia border, namely, LI and MA) are first extracted using different kinds of edge extraction algorithms [13]. Then, the distance of the two borders can be calculated to obtain IMT. As comprehensively reviewed in [13] and [14], algorithms based on various frameworks have been intended for segmentation of intima-media borders in ultrasound

images in the past two decades. Different methods are used for this task, such as edge detectors [9], [15], dynamic programming [12], [16], [17], snakes [8], [16], [18]–[22], and neural networks [23]. Among them, the snake algorithm is able to deform the contours using external and internal forces, which resultantly yield a smoothed curve [24]. Its tension and stiffness are beneficial for LI/MA segmentation because these profiles are always regular and continuous in the aspect of physiology [21].

Since snakes are sensitive to the initial contours, it should be initialized near to the correct IM borders when segmenting each frame in the sequence. Based on this understanding, the state-space approach is commonly used for the initialization of the snake in consecutive frames, namely, the IM border position is the state variable of the state-space equations, and is initialized using the results of the previous frame when segmenting an arbitrary frame in an ultrasound sequence [25], [26]. The Kalman filter and the H_∞ filter are common solutions of the state-space equations [27], [28].

Based on this strategy, we have developed an algorithm under the state-space framework [29]. An adaptive snake method is used to provide an accurate and robust measurement. Grayscale and derivative information of the first frame can help the snake be aware of the characteristics (image grayscale, image noise, IM border curvature, and movement in consecutive frames) of the sequence, so the parameters of the algorithm do not need to be adjusted when segmenting sequences of different characteristics. This work can accurately and robustly segment ultrasound sequences providing the first frame is properly manually segmented. The aim of the present study is to extend our previous work to a fully automatic scheme to segment the IM borders from ultrasound sequences of different characteristics. Firstly, a dynamic programming algorithm is introduced to automatically segment the first frame of the sequence. Then, a snake algorithm is performed to segment the remaining frames. The parameters of the snake are automatically adjusted according to the segmentation results of the first frame. For any other frame in the sequence, the *a priori* state estimate is used to initialize the snake positions, and the IM border positions are successively obtained under the state-space framework. The performance of our method has been evaluated in 62 patients' carotid ultrasound image sequences as well as and 3 synthetic sequences. The parameters are kept unchanged during the whole experiment. In order to fully evaluate our method, we used ultrasound sequences with various characteristics. The segmentation of the sequences is fully automatic, nevertheless, the user may choose to perform manual modification if they prefer.

II. METHODOLOGY

A. AUTOMATIC INITIALIZATION OF THE FIRST FRAME

The pre-processing procedure of ultrasound sequences are the same as in our previous work. The grayscale of each frame is firstly normalized into [0, 255], and then a Gaussian low-pass filter is applied in every frame. Then, the first image is processed as follows:

1) COARSE CLIPPING

To approximately locate the IM borders of each column in an image, we use the fact that carotid intima-media ultrasound images are dark (grayscale$<$10) inside the carotid lumen and bright (grayscale$>$180) inside the adventitia tunica [34]. For each column, we carried out a grayscale search. If N_1 (set to be 30 in our experiments) consecutive points are found to be dark (the grayscale of all these points are less than 10), we would take these points as the vessel lumen. Hence, the last point whose grayscale is less than 10 is chosen to be the upper bond of the LI border, and the y coordinate of this point is denoted as A_i. The actual location of LI is intuitively thought to be near to but lower than A_i. Then, the grayscale search continues until the brightest point is found. If the distance from this point to A_i is smaller than a threshold (50 in our experiments), this point is thought to be the lower bound of the MA border, and the y coordinate of this point is denoted as B_i. The actual location of MA is intuitively thought to be near to but higher than B_i. For ultrasound images with lumen noise, there may not exist N_1 consecutive points whose grayscales are less than 10. In this case, B_i is firstly determined using the above mentioned method, and then A_i is set to be the y coordinate of B_i minus 50 (because the IMT value is empirically smaller than 50 pixels). The areas upper to A_i and lower to B_i are set to be ban zones, which means that the front propagation of the dynamic programming (as will be discussed later) would not pass through these zones. In this way, the ultrasound image is coarsely clipped and the region of interest (ROI) is located. The LI and the MA borders are also distinguished from each other by grayscale.

2) SEED POINT GENERATION

The image gradient map is calculated in the y direction, and then the cost map C for dynamic programming is defined to be opposite number of the image gradient map. The values of the points in the ban zones are modified to be large value (for example, the general value of the gradient map in the ROI is ~ -100, so the values in the ban zones are set to be 500) to force the propagation path to leave these zones. After modifying the gradient map, we searched for the minima of the cost map for 30 columns from the left of the image. These minima constitute a valley in the feature map. Then, the linkage of the valley is checked from the first column. If the y coordinate of the minima in the neighboring columns differs by less than 2 pixels, these two columns are thought to be connected, and the length of the valley is increased by one. Lastly, the total length of the valley is examined. If the total length is larger than 10, then these minima are confirmed to be the borders, and the first minima is selected to be the seed point. Otherwise, the outliers of these 30 minima are deleted by setting the cost map value of these points to be large (500), and the second smallest point of the corresponding column is used to constitute the valley. Then the linkage is check

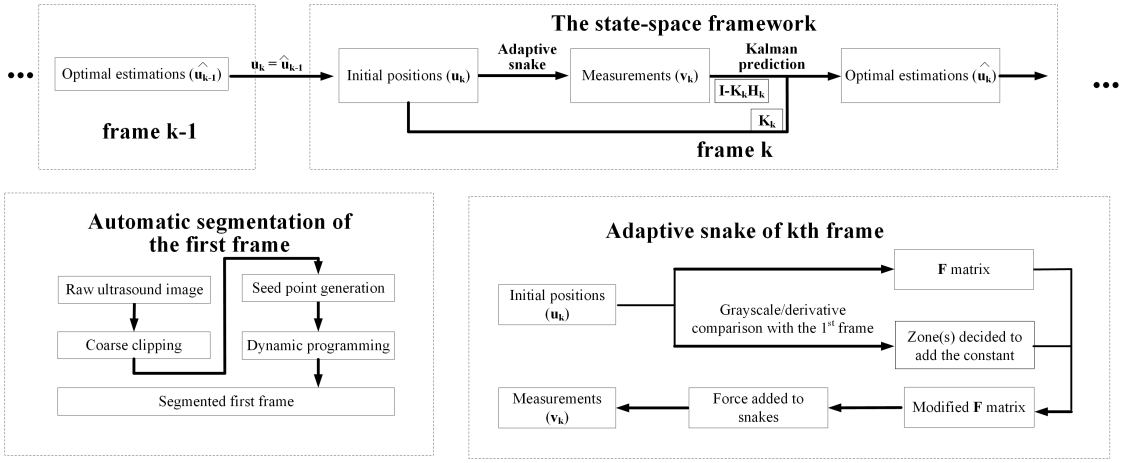

FIGURE 1. The flowcharts of our method. (1) The upper part illustrates the state-space framework: the results of the previous frame is used to initialize the snake of the current frame, and the results of the snake is considered to be the measurements. K_K and H_k are solved using the Kalman filter. Then the final segmentation of the current frame is calculated by a weight sum of the initial estimation and the measurements. (2) The left lower part illustrates the automatic segmentation of the first frame: the first frame is clipped by grayscale to get a rough position of the LI and MA border. Then the seed point is generated using the cost map. Lastly the segmentation of the first frame is performed by the dynamic programming using the seed point and the cost map. (3) The right lower part illustrates the adaptive snake algorithm.

anew until the valley is long enough and the seed point is determined. The y coordinate of the seed point is denoted as y_0, so the coordinates of this point is $(1, y_0)$.

3) DYNAMIC PROGRAMMING

A front propagation scheme is performed from the seed point to build a cumulative cost map C_c. The initial cost map is set to be the cost map value of the seed point:

$$C_c(1, y_0) = C(1, y_0) \tag{1}$$

Then, the cumulative cost map C_c is iteratively built from left (the seed point) to right for each column using the following equation (where x denotes the x coordinate of a point) [30]:

$$C_c(x, y_j) = \min_{i=-2,-1,0,1,2} \{C_c(x-1, y_{j+i}) + C(x-1, y_{j+i})\} \tag{2}$$

Equation (2) means that the cumulative cost map of the j^{th} point of the x^{th} column is the minimum of the cumulative cost map of the neighboring points (which means that the difference of y coordinate is less than 2) of its previous column plus the cost map of the corresponding points (which is similar to the partial path cost). Because the cost map reaches its minimum where the image gradient is the strongest, the cumulative cost map also reaches its minimum where the total image gradient along the propagation path is strongest. Moreover, in order to keep the smoothness of the segmented borders, the maximum deviation of y coordinate between two consecutive columns is set to be 2. Finally, when the propagation reaches the right side of the image, the point whose cumulative cost map is smallest is found and the minimal path is determined by back-tracking the points from the right side of the image to the seed point. The points on the minimal path are then thought to be the IM borders of the ultrasound images. The automatic initialization procedure is shown in the left lower part of Fig. 1.

B. THE SPACE-STATE FRAMEWORK FOR IMAGE SEQUENCE SEGMENTATION

The state-space approach is used to leverage the temporal consistency for image sequence segmentation. The fundamental of the state-space approach is the space-state equations (3):

$$\begin{aligned} \mathbf{x_n} &= \mathbf{F_{n-1}x_{n-1}} + \mathbf{q_{n-1}} \\ \mathbf{y_n} &= \mathbf{H_{n-1}x_{n-1}} + \mathbf{r_{n-1}} \end{aligned} \tag{3}$$

with the frame index n, the state variable $\mathbf{x_n}$, observation variable $\mathbf{y_n}$, system noise $\mathbf{q_{n-1}}$, observation noise $\mathbf{r_{n-1}}$ and the coefficient matrices $\mathbf{F_{n-1}}$ and $\mathbf{H_{n-1}}$. The goal of the state-space approach is to use the noisy observation $\mathbf{y_n}$ (which is the result of the snake algorithm) and the state variable $\mathbf{x_{n-1}}$ (which is the IM border positions of the previous frame) in the previous instant to determine its optimal estimate in the current instant. Since the purpose of this work is to make the segmentation framework automatic, we use Kalman filter to solve the state-space equations for speeding up computation. In Kalman filter, the state variable $\mathbf{x_n}$ of the current instant can be calculated by that of the previous instant $\mathbf{x_{n-1}}$ as well as the observation variable $\mathbf{y_n}$ using equations (4).

$$\begin{aligned} \mathbf{x_{n,prior}} &= \mathbf{F_{n-1}x_{n-1}} \\ \mathbf{P_{n,prior}} &= \mathbf{H_{n-1}P_{n-1}H_{n-1}}^T + \mathbf{Q_{n-1}} \\ \mathbf{K_n} &= \mathbf{P_{n,prior}H_n}^T(\mathbf{H_nP_{n,prior}H_n}^T)^{-1} + \mathbf{R_{n-1}} \\ \mathbf{x_n} &= \mathbf{x_{n,prior}} + \mathbf{K_n}(\mathbf{y_n} - \mathbf{H_nx_{n,prior}}) \\ \mathbf{P_n} &= (\mathbf{I} - \mathbf{K_nH_n})\mathbf{P_{n,prior}} \end{aligned} \tag{4}$$

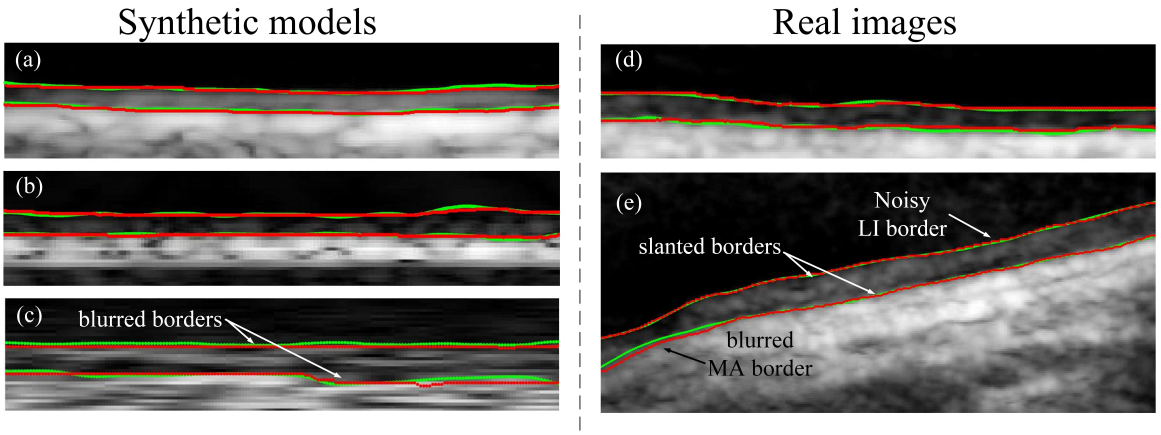

FIGURE 2. The segmentation results of some sample images in the sequences. The red lines represent the reference contours segmented by the physician, and the green lines represent the results of our segmentation method. The borders in (a)(b)(d) are comparatively clear, but those in (c)(e) are blurred. Moreover, the borders in (e) are slanted. It can be seen that the deviation of the segmentation results from the ground truth is small in all these figures.

Where the variables with subscript prior means the *a priori* variables at instant n, $\mathbf{Q_{n-1}}$ is the covariance matrices of the process noise $\mathbf{q_{n-1}}$, $\mathbf{R_n}$ is the covariance matrices of the process noise $\mathbf{r_n}$. Using these equations, the dynamics of variable $\mathbf{x}$ (IM border positions) and error covariance matrix $\mathbf{P}$ with respect to time (frame index) can be solved iteratively. The state-space framework is shown in the upper part of Fig. 1.

C. THE ACQUISITION OF MEASUREMENTS

The observation variable $\mathbf{y_n}$ is obtained using the snake algorithm. The snake is a set of points geometrically represented by the spatial coordinates u (u means the x or y coordinate of one point in the snake). The snake is pushed to the regions with strong image gradient by minimizing the snake energy, which is defined as:

$$E_{snake} = \sum_{i=1}^{N} \mathbf{G}(u_i) + \sum_{i=1}^{N} \left[\frac{\alpha_i}{2}(u_i - u_{i-1})^2 + \frac{\beta_i}{2}(u_{i+1} - 2u_i + u_{i-1})^2 \right] \quad (5)$$

where subscript i means the i^{th} point of the snake, α_i and β_i indicate the weight factors of lines, edges, elasticity and rigidity of the snake. $\mathbf{G}$ is the external energy field, a weighted sum of energies of lines and edges. If the initial snake $u_{i,0}$ is properly defined, then the snake can conform to the local minima of $\mathbf{G}$ (the edges of the images), achieving the segmentation of one figure.

In order to deal with speckle noise and large movements between successive frames, the snake algorithm is adjusted using the grayscale and derivative information of the neighboring points of each point in the snake. The main idea is to maintain a relatively constant grayscale and derivative. If the grayscale and derivative changes too much, an additional external force is added to push the snake back to the correct position, as detailed in [29].

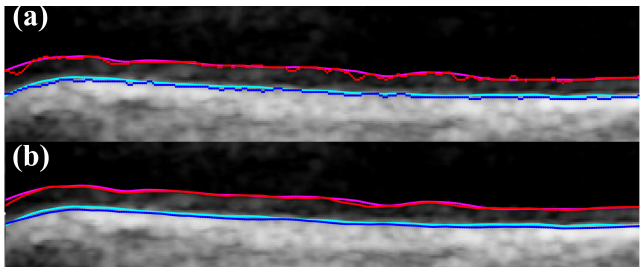

FIGURE 3. The segmentation of the first frame(red and blue lines for LI and MA) compared with the ground truth (pink and cyan lines for LI and MA). (a) before smoothing using Savitzky-Golay filter, (b) after smoothing using Savitzky-Golay filter.

III. EXPERIMENTS AND RESULTS

A total of 3 synthetic models and 62 subjects are enrolled in our study. The synthetic sequences are generated from the toolbox for *in silico* evaluation of motion estimators for the arterial wall, developed by the BioSim Laboratory of the National Technical University of Athens [31]. For the real subjects, an ultrasound physician collected all the carotid ultrasound data by using one ultrasound system iU22 (Philips Ultrasound, Bothell, WA, USA) with a 7.5MHz liner array transducer. We ran our program on Matlab 2015B in a desktop computer with Intel(R) Core(TM) i5-5200U CPU (2.20GHz) and 8GB RAM.

The manual segmentation results of every frame in all the 65 sequences are performed by 3 ultrasound physicians blinded to the other results. Specifically, the first physician performed the manual delineation twice with a time interval of 1 month. The average of the 4 results are considered as the ground truth. Four criteria are used for accuracy and robustness evaluation of our segmentation method.

A. THE MEAN ABSOLUTE ERROR (MAE)

Fig. 2 is the segmentation results for different image sequences. Fig. 2(a)∼(c) represents images from the

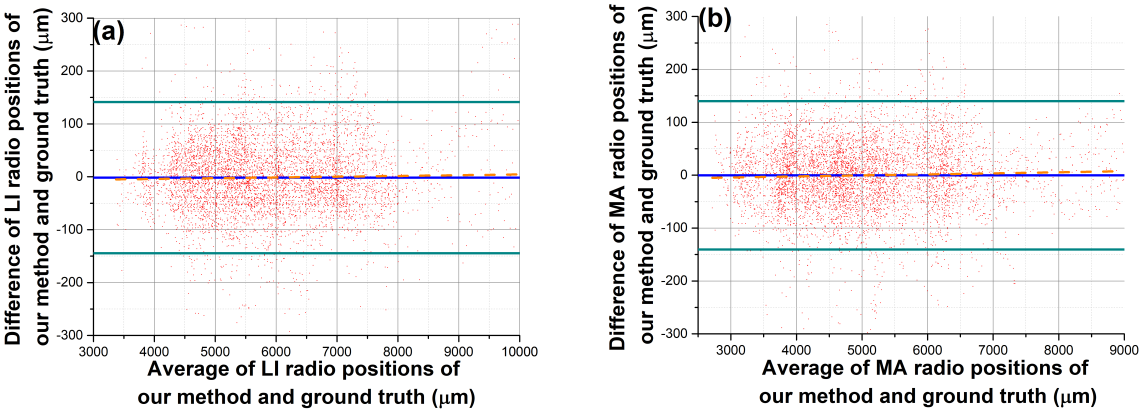

FIGURE 4. Bland-Altman plot for LI(a) and MA(b) segmentation. The blue lines represent the mean discrepancy of our results and the manually delineated results. The intervals between cyan lines are the 95% confidence interval. The linear fittings of the points in the BA plot are shown by the red dashed lines, which shows that the difference of our approach and the ground truth is independent of their average. These results prove that the accuracy of our method is high.

synthetic models, while Fig. 2(d)∼(e) represents those from the clinical models. It is illustrated that when the borders are clear, our segmentation results nearly coincide with the ground truth (Fig. 2(a), (b), (d)). Even for synthetic or real images that are blurred (Fig. 2(c)) or effected with noise (Fig. 2(e)), the segmentation error is rather small. The mean error for the 3 synthetic models are: (LI) 0.586 ± 0.694 pixel, (MA) 0.569 ± 0.745 pixel. The mean error for the 62 real sequences are: (LI) 0.615 ± 0.720 pixel ($32.1 \pm 37.5\mu$m), (MA) 0.672 ± 0.796 pixel ($35.0 \pm 41.5\mu$m).

B. MAE OF THE FIRST FRAME

In order to test the results for automatic segmentation, we also calculated the MAE of the first frame. The mean error for the 3 synthetic models are: (LI) 0.591 ± 0.732 pixel, (MA) 0.608 ± 0.813 pixel. The mean error for the 62 real sequences are: (LI) 0.631 ± 0.746 pixel ($32.9 \pm 38.8\mu$m), (MA) 0.704 ± 0.826 pixel ($36.7 \pm 43.0\mu$m). The MAE of the first frame is slightly larger than that of all images. This is probably because the results of the dynamic programming is not as smooth as that of the snake. Although the results can be smoothed using various filters (such as average filter, median filter, and Savitzky-Golay filter), the smoothing procedure causes the segmented results to move in the y direction. This may result in a slightly larger error in the first frame (as shown in Fig. 3). Luckily, as demonstrated in [29], slight deviation of the initial contour from the ground truth does not severely affect the results of the segmentation of the following frames.

C. THE BLAND-ALTMAN PLOTS

As shown in Fig. 4, the plot consists of over 40000 points from over 2900 frames in 62 sequences, and illustrates the deviation between our approach and the ground truth to be -1.45μm for LI and -0.38μm for MA. The 95 % confidence intervals (dark cyan lines) are 141μm for LI and 139μm for MA. Also, the scattered points are linearly fitted, and the absolute value of the slopes of the fitted lines (black dotted lines) is less than 0.002 for LI and MA. This shows that the average discrepancies of our results and the manually delineated results do not rely on their average.

D. LINEAR REGRESSION ANALYSIS

The estimated IMT is also compared with reference tracings. For all the sequences, the linear regression analysis is performed to evaluate the relation of the estimated IMT with the ground truth. It can be seen in Fig. 5 that the IMTs that are obtained by our method is consistent with that of the ground truth. The R^2 value of the linear regression is 0.954.

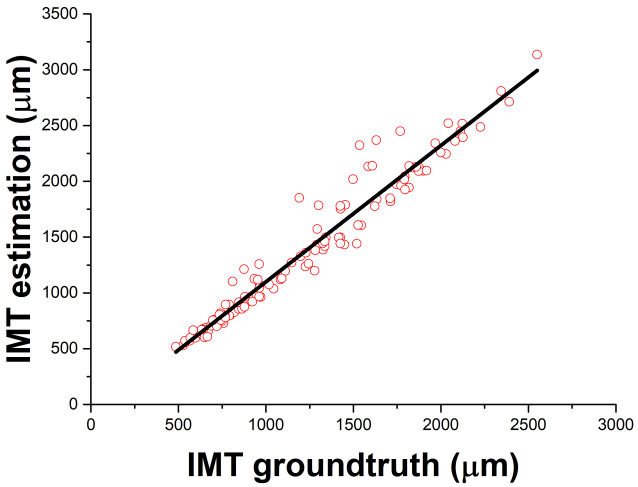

FIGURE 5. Linear regression of the IMT estimated by our method and the manual reference. The high R^2 value of the linear regression demonstrates the accuracy our segmentation method.

E. COMPARISON WITH OTHER METHODS

Our approach is compared with recent studies [32], [33]. These studies are respectively based on the dynamic programming method and the Chan-Vese method. Also, our results are compared with the inter-observer error between the first

and second physician, the inter-observer error between the first and third physician, and the intra-observer error of the first physician. It is shown in Fig. 6 that the accuracy of our method is higher than those of the other methods, and the average MAE of our method is on the same order of magnitude as the inter- and intra-observer error.

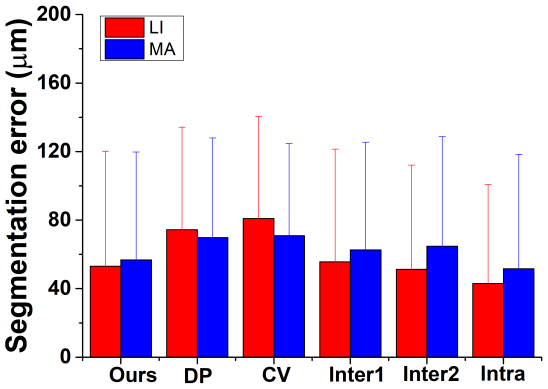

FIGURE 6. Comparative results of the segmentation error between our method, the dynamic programming method, the Chan-Vese method, the inter-observer errors, and the intra-observer error.

F. LIMITATIONS

The limitation of this work is that the Dynamic Programming method cannot deal with ultrasound images with plaques. This is because the nature of Dynamic Programming limits the difference of the y coordinates in consecutive columns. In this paper, we set the maximum difference to be 2 pixel. On one hand, this configuration prevents the effect of lumen noise, on the other hand, however, it causes error when the difference is really larger than 2 pixel (which may happen in sequences with plagues). However, if the difference tolerance is increased, sequences without plagues can be affected by lumen noise, resulting in a lower accuracy.

IV. CONCLUSION

In this paper, we propose a fully automatic method aiming at segmenting the IM borders from ultrasound image sequences. Firstly, the first frame of the sequence is segmented based on the dynamic programming approach, and the rest frames are segmented using the state-space framework with the help of the grayscale-derivative constraint snake. The evaluation of our method is performed using a total of 65 sequences. The MAE, BA plot, and the linear regression of the IMT estimated by our method and the manual reference show that our method can achieve high accuracy. Also, our method outperformed similar work using the popular dynamic programing and lever set algorithm. These results show the potential of our method for clinical usage.

ACKNOWLEDGMENT

(Shen Zhao and Guangrui Li contributed equally to this work.)

REFERENCES

[1] I.-K. Jang *et al.*, "Visualization of coronary atherosclerotic plaques in patients using optical coherence tomography: Comparison with intravascular ultrasound," *J. Amer. College Cardiol.*, vol. 39, no. 4, pp. 604–609, 2002.

[2] J. F. Polak, M. Szklo, and D. O'Leary, "Associations of coronary heart disease with common carotid artery near and far wall intima-media thickness: The multi-ethnic study of atherosclerosis," *J. Amer. Soc. Echocardiogr.*, vol. 28, no. 9, pp. 1114–1121, 2015.

[3] J. H. Stein and H. M. Johnson, "Carotid intima-media thickness, plaques, and cardiovascular disease risk: Implications for preventive cardiology guidelines," *J. Amer. College Cardiol.*, vol. 55, no. 15, pp. 1608–1610, 2010.

[4] C. Jarpa, V. Pineda, and C. Manterola, "Thickness of carotid intimamedia as a predictor of cardiovascular event. Systematic review of the literature," *Int. J. Morphol.*, vol. 31, no. 1, pp. 293–300, 2013.

[5] M. Skilton *et al.*, "Noninvasive measurement of carotid extra-media thickness: Associations with cardiovascular risk factors and intima-media thickness," *JACC, Cardiovascular Imag.*, vol. 2, no. 2, pp. 176–182, 2009.

[6] S. B. Nair, R. Malik, and R. S. Khattar, "Carotid intima–media thickness: Ultrasound measurement, prognostic value and role in clinical practice," *Postgraduate Med. J.*, vol. 88, no. 1046, pp. 694–699, 2012.

[7] L. Zhang *et al.*, "Evaluation of carotid artery elasticity changes in patients with type 2 diabetes," *Cardiovascular Diabetol.*, vol. 196, pp. 391–397, Feb. 2008.

[8] D.-C. Cheng, A. Schmidt-Trucksass, K.-S. Cheng, M. Sandrock, Q. Pu, and H. Burkhardt, "Automatic detection of the intimal and the adventitial layers of the common carotid artery wall in ultrasound B-mode images using snakes," in *Proc. Int. Conf. Image Anal. Process.*, vol. 21, 1999, pp. 452–457.

[9] F. Faita, V. Gemignani, E. Bianchini, C. Giannarelli, L. Ghiadoni, and M. Demi, "Real-time measurement system for evaluation of the carotid intima-media thickness with a robust edge operator," in *Proc. Int. Conf. IEEE Eng. Med. Biol. Soc.*, vol. 1, 2006, pp. 715–718.

[10] P. Holdfeldt, M. Viberg, and T. Gustavsson, "A new method based on dynamic programming for boundary detection in ultrasound image sequences," in *Proc. Int. Conf. IEEE Eng. Med. Biol. Soc.*, Aug. 2008, pp. 3072–3074.

[11] J. F. Polak *et al.*, "Changes in carotid intima-media thickness during the cardiac cycle: The multi-ethnic study of atherosclerosis," *J. Amer. Heart Assoc.*, vol. 1, pp. 301–306, 2012.

[12] G. Zahnd *et al.*, "A fully-automatic method to segment the carotid artery layers in ultrasound imaging: Application to quantify the compression-decompression pattern of the intima-media complex during the cardiac cycle," *Ultrasound Med. Biol.*, vol. 43, no. 1, pp. 239–257, 2017.

[13] F. Molinari, G. Zeng, and J. S. Suri, "A state of the art review on intima–media thickness (IMT) measurement and wall segmentation techniques for carotid ultrasound," *Comput. Methods Programs Biomed.*, vol. 100, no. 3, pp. 201–221, 2010.

[14] C. P. Loizou, "A review of ultrasound common carotid artery image and video segmentation techniques," *Med. Biol. Eng. Comput.*, vol. 52, no. 12, pp. 1073–1093, 2014.

[15] F. Molinari *et al.*, "Completely automated multiresolution edge snapper—A new technique for an accurate carotid ultrasound IMT measurement: Clinical validation and benchmarking on a multi-institutional database," *IEEE Trans. Med. Imag.*, vol. 21, no. 3, pp. 1211–1222, Mar. 2012.

[16] I. Wendelhag, Q. Liang, T. Gustavsson, and J. Wikstrand, "A new automated computerized analyzing system simplifies readings and reduces the variability in ultrasound measurement of intima-media thickness," *Stroke*, vol. 28, no. 11, pp. 2195–2200, 1997.

[17] R. Rocha, J. Silva, and A. Campilho, "Automatic detection of the carotid lumen axis in B-mode ultrasound images," *Comput. Methods Programs Biomed.*, vol. 115, no. 3, pp. 110–118, 2014.

[18] N. Santhiyakumari, P. Rajendran, M. Madheswaran, and S. Suresh, "Detection of the intima and media layer thickness of ultrasound common carotid artery image using efficient active contour segmentation technique," *Med. Biol. Eng. Comput.*, vol. 49, no. 11, pp. 1299–1310, 2011.

[19] D. Zhang, C. Wang, and S. Zhou, "New method of vessel centerline extraction from 3D CT coronary angiography based on open-snake," in *Proc. IET Int. Conf. Biomed. Image Signal Process.*, 2015, pp. 1–5.

[20] J. Wang and X. Li, "Guiding ziplock snakes with *a priori* information," *IEEE Trans. Med. Imag.*, vol. 12, no. 2, pp. 176–185, Feb. 2003.

[21] F. Molinari *et al.*, "Constrained snake vs. conventional snake for carotid ultrasound automated IMT measurements on multi-center data sets," *Ultrasonics*, vol. 52, no. 7, pp. 949–961, 2012.
[22] X. Xu, Y. Zhou, X. Cheng, E. Song, and G. Li, "Ultrasound intima–media segmentation using Hough transform and dual snake model," *Comput. Med. Imag. Graph.*, vol. 36, no. 3, pp. 248–258, 2012.
[23] R.-M. Menchón-Lara, M.-C. Bastida-Jumilla, J. Morales-Sánchez, and J.-L. Sancho-Gómez, "Automatic detection of the intima-media thickness in ultrasound images of the common carotid artery using neural networks," *Med. Biol. Eng. Comput.*, vol. 52, no. 2, pp. 169–181, 2013.
[24] M. Kass, A. Witkin, and D. Terzopoulos, "Snakes: Active contour models," *Int. J. Comput. Vis.*, vol. 1, no. 4, pp. 321–331, 1988.
[25] Z. Gao *et al.*, "Robust estimation of carotid artery wall motion using the elasticity-based state-space approach," *Med. Image Anal.*, vol. 37, pp. 1–21, Apr. 2017.
[26] Z. Gao *et al.*, "Motion tracking of the carotid artery wall from ultrasound image sequences: A nonlinear state-space approach," *IEEE Trans. Med. Imag.*, vol. 37, no. 1, pp. 273–283, Jan. 2018.
[27] D. Simon, *Optimal State Estimation*. Hoboken, NJ, USA: Wiley, 2006.
[28] H. Zhang, S. Tong, H. Liu, and P. Shi, "Simultaneous recovery of left ventricular motion and input forces from medical image sequences," in *Proc. IEEE Int. Symp. Biomed. Imag., Nano Macro (ISBI)*, Washington, DC, USA, Apr. 2007, pp. 380–383.
[29] S. Zhao *et al.*, "Robust segmentation of intima-media borders with different morphologies and dynamics during the cardiac cycle," *IEEE J. Biomed. Health Inform.*, Nov. 2017. [Online]. Available: https://ieeexplore.ieee.org/document/8116628/
[30] M. Sonka, V. Hlavac, and R. Boyle, *Image Processing, Analysis, and Machine Vision*, 3rd ed. Toronto, ON, Canada: Thomson Learning, 2008, ch. 6.2.4, pp. 197–211.
[31] G. Aimilia, D. Sofia, K. Vasileios, and N. Konstantina, "A toolbox for in silico evaluation of motion estimators for the arterial wall," in *Proc. Annu. Int. Conf. IEEE Eng. Med. Biol. Soc. (EMBC)*, Chicago, IL, USA, Aug. 2014, p. 1. [Online]. Available: https://www.researchgate.net/publication/280556378_A_Toolbox_for_in_silico_evaluation_of_motion_estimators_for_the_arterial_wall
[32] Y. Zhou, X. Cheng, X. Xu, and E. Song, "Dynamic programming in parallel boundary detection with application to ultrasound intima-media segmentation," *Med. Image Anal.*, vol. 17, no. 8, pp. 892–906, 2013.
[33] A. M. F. Santos, R. M. Santos, P. M. A. C. Castro, E. Azevedo, L. Sousa, and J. M. R. S. Tavares, "A novel automatic algorithm for the segmentation of the lumen of the carotid artery in ultrasound B-mode images," *Expert Syst. Appl.*, vol. 40, no. 16, pp. 6570–6579, 2013.
[34] C. P. Loizou, C. S. Pattichis, and M. Pantziaris, "Snakes based segmentation of the common carotid artery intima media," *Med. Biol. Eng. Comput.*, vol. 45, pp. 35–49, 2007.

SHEN ZHAO received the Ph.D. degree from Tsinghua University in 2015. He was with the Institute of Biomedical and Health Engineering, Shenzhen Institutes of Advanced Technology, Chinese Academy of Sciences, for two years. He is currently a Post-Doctoral Researcher with the Department of Medical Biophysics, The University of Western Ontario. His research interests include medical image processing, deep learning, and big data.

GUANGRUI LI received the B.S. degree in automation from Central South University, Changsha, China, in 2016. He is currently pursuing the master's degree in control engineering with Shandong University, Jinan. His research interests include medical image processing and pattern recognition.

WEI ZHANG (S'06–M'11) received the Ph.D. degree in electronic engineering from The Chinese University of Hong Kong in 2010. He is currently a Professor with the School of Control Science and Engineering, Shandong University, China. He has authored over 60 papers in international journals and refereed conferences. His research interests include computer vision, image processing, pattern recognition, and robotics. He served as a program committee member and a reviewer for various international conferences and journals in image processing, computer vision and robotics.

JIANJUN GU received the Ph.D. degree from the Department of Electrical and Computer Engineering, University of Alberta, Edmonton, AB, Canada. He is currently an Adjunct Professor with the School of Control Science and Engineering, Shandong University, China. His research interests include image processing, biomedical engineering, and robotics. He is currently an Associate Editor of the *Journal of Control and Intelligent Systems*, the *International Journal of Robotics and Automation*, the IEEE TRANSACTIONS ON MECHATRONICS, the IEEE ACCESS, and the *IEEE SMC Magzine*.